Vol 16 No 9, September 2007
1009-1963/2007/16(09)/2745-07

Chinese Physics

Noninvasive temperature estimation by detecting echo-strain change including thermal expansion*

Ma Yong(马 勇), Zhang Dong(章 东)†, Gong Xiu-Fen(龚秀芬), Liu Xiao-Zhou(刘晓宙), Ma Qing-Yu(马青玉), and Qiu Yuan-Yuan(邱媛媛)

Institute of Acoustics, Key Laboratory of Modern Acoustics, Nanjing University, Nanjing 210093, *China*

(Received 29 July 2006; revised manuscript received 14 January 2007)

This article studies the feasibility of noninvasive temperature estimation by detecting echo-strain including thermal expansion in therapeutic ultrasound treatment. This technique evaluates distributions of echo-strain and temperature inside the tissue by detecting echo signals pre- and post-heating, in combination with the temperature dependence of sound speed and thermal expansion. In the computer simulation and experimental study, echo signals pre- and post-heating are acquired and then the temperature elevation is evaluated by correlation analysis. Results demonstrate that this technique can effectively extend the measured temperature range up to 75°C with an accuracy of ±2 °C.

Keywords: echo-strain, noninvasive temperature estimation, therapeutic ultrasound
PACC: 4335, 8750C

1. Introduction

Ultrasound provides an excellent means of delivering energy to accessible treatment volumes, and many ultrasound-based therapeutic procedures have been developed and used clinically, including blood–brain barrier disruption, hyperthermia, tissue thermal ablation and high intensity focused ultrasound.[1,2] Despite the usefulness and great potential of these procedures, many disadvantages have limited their acceptance for widespread use. As a thermal-induced technique, therapeutic ultrasound is required to accurately deliver ultrasound energy into the target and precisely control the temperature increase. Consequently, it is essential to establish a real-time noninvasive technique to monitor the temperature rise in the treatment. In the past years, several techniques have been developed for noninvasive estimation of temperature change in ultrasound therapy.[3] Most of them are based on magnetic resonance imaging (MRI) and diagnostic ultrasound. MRI possesses high spatial resolution and provides good accuracy of temperature detection. But its poor temporal resolution limits its real-time detection.[4] In comparison with MRI, ultrasound-based methods for temperature monitoring are less expensive and easier to implement by integrating a probing transducer in a therapeutic ultrasound system. Especially, the noninvasive technique for detecting time-shift of echoes has been investigated by many researchers, and demonstrated to be an effective tool in temperature monitoring.[5−9] Temperature-related variations in the speed of sound (SOS) induce a variation in the time of flight of received echoes. The variation in SOS can be estimated by using correlation algorithm between two echo signals acquired before and after heating. Accordingly, temperature elevation can be evaluated based on the hypothesis of the linear relationship between SOS and temperature. However, the curve of SOS versus temperature in biologic tissues was observed to be parabolic, and that the little variation in SOS around the maximum resulted in low sensitivity at monitoring temperature higher than 60 °C.[10] Moreover, the current technique does not consider the significant variation in thermal expansion[11] due to the stiffening of tissues induced by the thermal effect during therapeutic ultrasound treatment.

This paper introduces a parameter called echo-strain to represent both time-shift variation and waveform distortion in echoes. We study the feasibility of evaluating temperature change by detecting echo-strain in combination with the temperature dependence of SOS and thermal expansion. In the computer simulation, the echo signals pre- and post-heating are

*Project supported by the National Natural Science Foundation of China (Grant No 10474044) and the Program for New Century Excellent Talents in University of China (CNCET).
†E-mail: dzhang@nju.edu.cn

first simulated on the basis of the calculated temperature distribution during heating; then the temperature elevation inside tissues is estimated by using correlation analysis of these echo signals and combining with both the temperature dependence of SOS and thermal expansion. Furthermore, a preliminary experiment is performed by using the liver tissue heated in a temperature-controlled water bath. The measured echo signals are acquired during heating, and the temperature variation inside the tissue is reconstructed with the echo-strain parameter.

2. Principle and method

2.1. Time-shift and echo-strain

Consider a scatterer at an axial depth z away from the surface of the transducer. The transit time of the pulse-echo from the scatterer is

$$t(z) = 2\int_0^z c_0^{-1}(x)\mathrm{d}x, \tag{1}$$

where $c_0(x)$ is the SOS at depth x at temperature T_0. After therapeutic ultrasound irradiation, the temperature rises and the transit time of the pulse-echo at x is changed to

$$t'(z) = 2\int_0^z (1+\alpha_{\mathrm{T}}\Delta T_x)c^{-1}(x)\mathrm{d}x, \tag{2}$$

where α_{T} is the linear coefficient of thermal expansion of the propagating medium. $\Delta T_x = T_x - T_0$ represents the temperature rise at depth x. $c(x)$ is the SOS at depth x at temperature T_x. Combining Eqs.(1) and (2), we obtain the time-shift of pre- and post-heating echoes caused by the scatterer at z,

$$\begin{aligned}\delta t_z &= t'(z) - t(z)\\ &= 2\int_0^z [(1+\alpha_{\mathrm{T}}\Delta T_x)c^{-1}(x) - c_0^{-1}(x)]\mathrm{d}x.\end{aligned} \tag{3}$$

The relationship between SOS and temperature in biologic tissues can be deduced by the mixture law.[12] Generally, the biologic tissue is supposed to be composed of water, fat, and residue (proteins, carbohydrates and so on). Therefore, the temperature-dependent SOS is

$$C^{-1}(T) = x_{\mathrm{w}}C_{\mathrm{w}}^{-1}(T) + x_{\mathrm{f}}C_{\mathrm{f}}^{-1}(T) + x_{\mathrm{r}}C_{\mathrm{r}}^{-1}(T), \tag{4}$$

where x_{w}, x_{f} and x_{r} represent the volume fractions of water, fat, and residue respectively. $C_{\mathrm{w}}(T)$, $C_{\mathrm{f}}(T)$, and $C_{\mathrm{r}}(T)$ indicate the SOS of each component. Figure 1 shows the temperature dependence of SOS in liver tissues by using Eq.(4), where x_{w}, x_{f}, and x_{r} are 76.33%, 3.61%, and 20.12% respectively.[6]

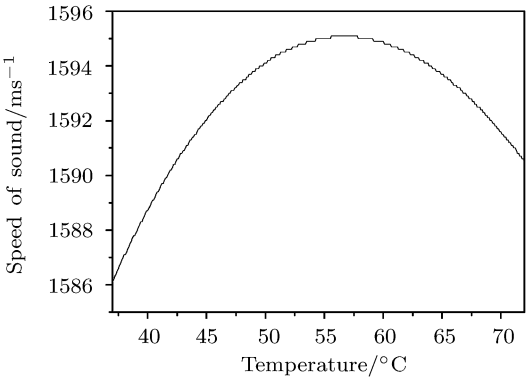

Fig.1. Temperature dependence of SOS in liver tissue.

The variation of strain due to the changes of SOS and thermal expansion induced by heating is expressed as

$$s(z) = \frac{1}{2}C_0(z)\frac{\partial \delta t_z}{\partial z} = \frac{(1+\alpha_{\mathrm{T}}\Delta T_z)C_0(z)}{C(z)} - 1. \tag{5}$$

Figure 2 shows the temperature-dependent echo-strain in liver tissues obtained using Eq.(5), where $\alpha_{\mathrm{T}} = 120\times10^{-6}\,^{\circ}\mathrm{C}^{-1}$ for normal liver tissue.

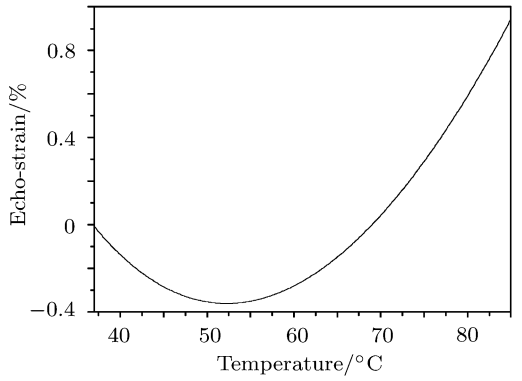

Fig.2. Temperature dependence of echo-strain in liver tissue.

2.2. Temperature estimation by echo signals

Assuming that the echo signals pre- and post-heating are $f_1(t)$ and $f_2(t)$ corresponding to temperatures T_0 and $T_0+\Delta T$ respectively. The time-shift $\delta_{\mathrm{inv}}t$ of $f_2(t)$ with reference to $f_1(t)$ is given by the maximum Δt in the cross-correlation function in Eq.(6):[9]

$$R_{f_1f_2}(\Delta t) = E[f_1(t)\cdot f_2(t+\Delta t)], \tag{6}$$

where $E[\,]$ represents the mathematic expectation.

Considering the linear property of imaging system, the spatial displacement δz_z of the tissue element is given by the temporal displacement induced by heat.

$$\delta z_z = c_0 \delta t_z / 2, \tag{7}$$

where c_0 is the sound speed at 37 °C.

The cumulated time-shift by the scattering region from axial depths z' to z is

$$\tau_z = 2 \int_{z'}^{z} [(1 + \alpha_{\mathrm{T}} \Delta T_x)/c(x) - 1/c_0(x)] \mathrm{d}x. \tag{8}$$

By means of Eq.(5), the average inversed echo-strain in this region is given by

$$s_{\mathrm{inv}}(z) = \frac{C_0(z)}{2} \frac{\partial \delta_{\mathrm{inv}} t_z}{\partial z} = \frac{C_0(z)}{2} \frac{\tau_z}{z - z'}. \tag{9}$$

In combination with the temperature dependence of echo-strain in Fig.2, we can determine the temperature rise induced by the heat.

3. Computer simulation

The schematic cross-section of the model for noninvasive temperature estimation is shown in Fig.3. An annular sphere therapeutic ultrasound transducer with an outer radius of 11.79 mm and a focal length of 35 mm operates at its central frequency of 3.5 MHz. A circular focusing transducer with a radius of 3mm and a central frequency of 7.5 MHz, is embedded with the therapeutic transducer coaxially and con-focally used as the receiver.

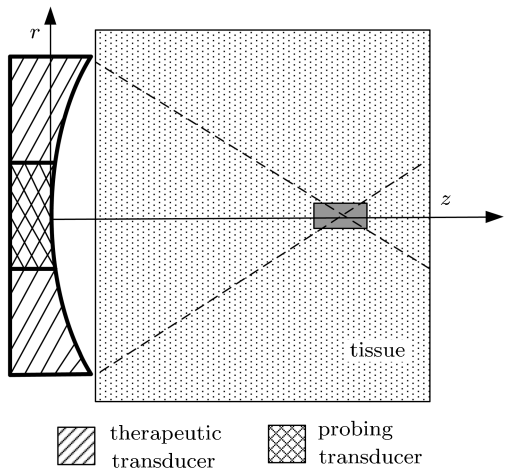

Fig.3. Cross-section of model in a cylindrical coordinates system.

For the purpose of the temperature estimation, the pre- and post-heating echo signals are required for correlation analysis. To simulate those echo signals, we performs the following steps: 1) the nonlinear acoustic field radiated from the therapeutic transducer is simulated using the nonlinear Khokhlov–Zabolotskaya–Kuznetsov (KZK) equation,[13,14] 2) the in situ temperature distribution is computed by using Pennes equation,[15,16] 3) the time-shift distribution is obtained in combination with the temperature dependence of SOS and thermal expansion, and 4) the echo signal is simulated based on the time-shifts of scatters.

In the numerical computation, parameters in the KZK equation are given as follows: frequency is 3.5 MHz, pressure of sound resource is 248.3 kPa, SOS in liver tissue at 37 °C is 1586 m/s, density of liver tissue is 1100 kg/m^3, and the attenuation coefficient of the nth harmonic is $4.5(nf/f^*)^{1.1} Np/m$ with $f^* = 1$ MHz. In Pennes equation, the perfusion rate (cooling by blood flow) is 0.5 kg/(m^3·s), the thermal conductivity of the tissue is 0.6 W/(m·K), heat capacities of the tissue and the blood are both 3800 J/(kg·K), and the ambient temperature in the tissue is 37 °C. Numerical solutions for KZK and Pennes equations are based on the implicit backward finite difference algorithm. The initial normalized axial and radial step-sizes are 10^{-4} and 10^{-3} (normalized by the focal depth and the outer radius of therapeutic transducer respectively). Regarding the compromise between computation accuracy and time-consuming, we let the axial step-size be modulated along with increasing axial depth and reach a minimum at the focus.

Figure 4(a) shows the distribution of temperature increase within the tissue after 2s heating. On the basis of the SOS-temperature relationship as displayed in Fig.1, we obtain the SOS distribution as shown in Fig.4(b). Obviously, the SOS distribution shows its correlation with temperature distribution, but with low sensitivity near the focus.

From the SOS distribution in Fig.4(b) and Eq.(3), we can assess the time-shift distribution as shown in Fig.5(a). To make a comparison with the case without considering thermal expansion of the tissue, we set $\alpha_{\mathrm{T}} = 0$ in Eq.(3) and obtain the time-shift distribution as shown in Fig.5(b). From the comparison, we find that thermal expansion of the tissue contributes a lot to the time-shift. For example, the time-shift at the focus in Fig.5(b) is higher about 20 ns (50%) than that in Fig.5(a).

From the time-shifts in Fig.5 and Eq.(7), we can evaluate the distribution of scatterer displace-

ment. Before therapeutic ultrasound irradiation heating, scatterers are set to have a Gaussian random distribution. After heating, these scatterers move axially. Based on the displacement of scatter induced by therapeutic ultrasound thermal effect, we can update the position of the scatterer, and thereby simulate echo signals received by the probing transducer. In this paper, Field II[17,18] is utilized to simulate echo signals pre- and post- heating, where the density of scatterers is 160/mm^3[18] in a region 0.5mm×0.5mm×1 mm, the transmitting signal is a 7.5 MHz sine wave with 1.5 cycles and Hanning apodization, and the received signal is sampled at 200 MHz.

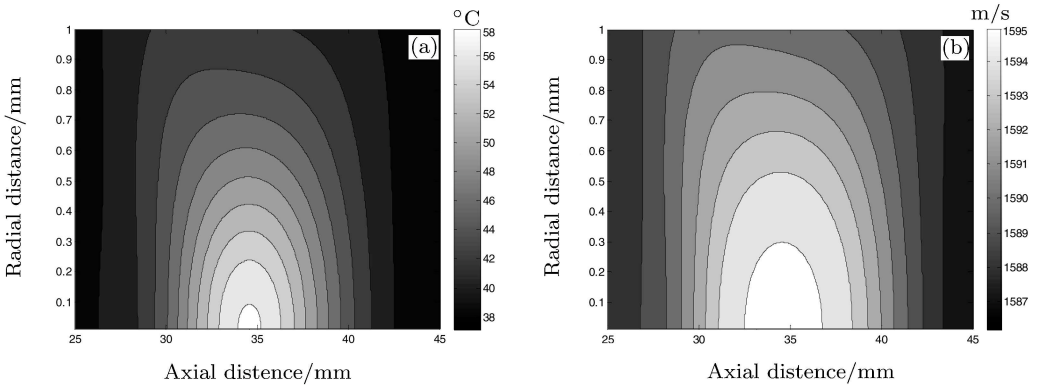

Fig.4. (a) Distribution of temperature and (b) distribution of SOS.

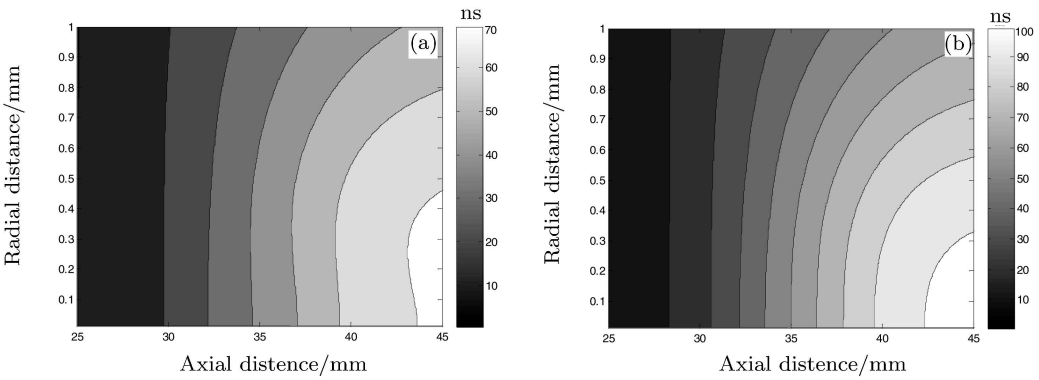

Fig.5. Distributions of time-shift for (a) SOS + thermal expansion and (b) SOS only.

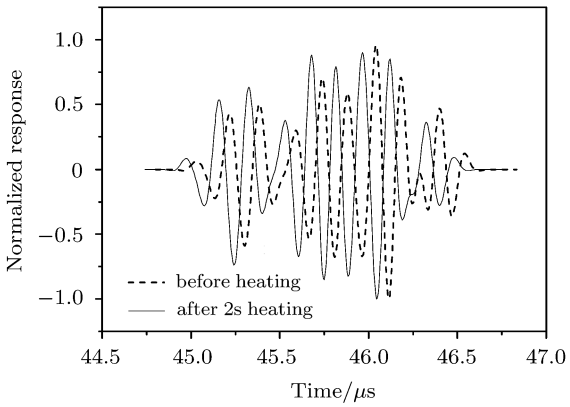

Fig.6. Simulated echo signals from the scattering region around the focus.

Figure 6 shows echo signals from the scattering region, the centre of which is located at the focus. The dashed line represents the pre-heating echo signal, and the solid line indicates the echo signal after 2s heating. In addition, due to the difference of time delays, we can find the distortion of waveform after heating.

From the post- and pre-heating echo signals and Eq.(6), we deduce the time-shift inversely as shown in Fig.7, where the solid and dashed lines indicate distributions of the time-shift with and without considering the thermal expansion of the tissue, respectively. We find that when considering the thermal expansion, the time-shift rises more rapidly in the focal region from 25 to 45 mm, where the corresponding high temperature is observed in Fig.4(a).

By analysing the inverse time-shifts described by

Eqs.(8) and (9), we can evaluate the axial distribution of echo-strain after heating. On the basis of the temperature dependence of the echo-strain, we can reconstruct the axial temperature distribution as shown in Fig.8. For comparison, the result obtained according to the SOS-temperature relationship is also plotted in this figure. We can find that the inverse temperature distribution by echo-strain including thermal expansion is more close to the theoretical prediction, especially in the focal region. The discrepancy between the theoretical prediction and the measured result obtained from the temperature dependence of SOS is due to the fact that SOS is not sensitive to temperature in the region from 52 to 62 °C.

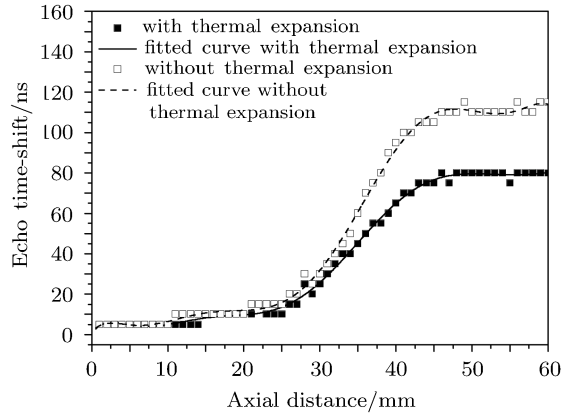

Fig.7. Axial distribution of the inversed time-shift.

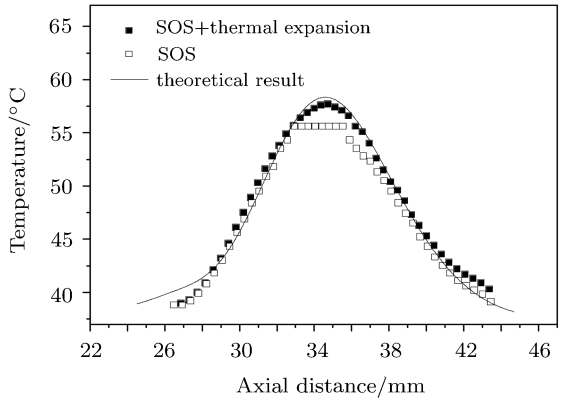

Fig.8. Axial distribution of estimated temperature.

4. Experiment and discussion

In order to demonstrate the feasibility of the method presented in this paper, we have conducted a preliminary experiment, in which the liver tissue specimen is heated using a temperature-controlled water bath while echo signal is acquired using a focusing transducer. The experimental setup is shown in Fig.9. A 20 mm diameter, circular concave transducer (Panametrics V304, centre frequency 5 MHz, focal length 50 mm, USA) is used for both emitting and receiving ultrasound signals. A computer-controlled pulser/receiver (Panametrics 5900PR, USA) is used to drive the probing transducer and a digital oscilloscope (Agilent 54810, USA) is used to acquire the echo signals at a sampling frequency of 250 MHz. The fresh porcine liver tissue sample is packed into a cylindrical sample holder with a thickness of 20 mm for vitro experiments. The sample holder is submerged in the water and positioned at the focus of the transmitter. A piece of sound absorbing material is located behind the sample to avoid the multi-reflection effect. The temperature-controlled water bath is used to raise the temperature of the specimen by 5 °C over a period of 20 minutes.

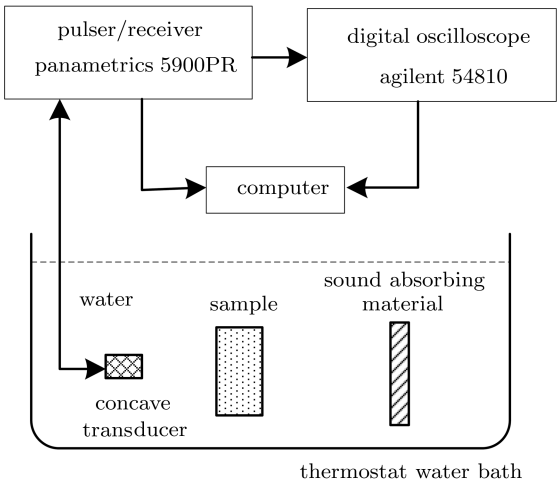

Fig.9. The schematic diagram of experimental setup.

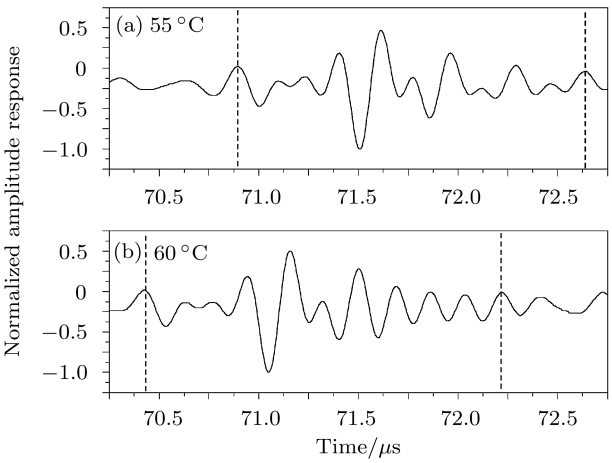

Fig.10. Echoes from the scattering region near the focus at (a) 55 °C and (b) 60°C.

Figure 10 shows echo signals from the scattering region around the focus at 55 and 60 °C, where the echo signal at 60 °C is shift forward as compared with that at 55 °C. It suggests that a 5 °C temperature rise can be easily tracked by observing the time shift of the signal. Compared with the echo transmitting time at 37 °C, we obtain the relationship between temperature and echo time-shift shown in Fig.11, where the theoretical prediction is given by Eq.(3) with $\alpha_{\mathrm{T}} = 120 \times 10^{-6\circ}\mathrm{C}^{-1}$.

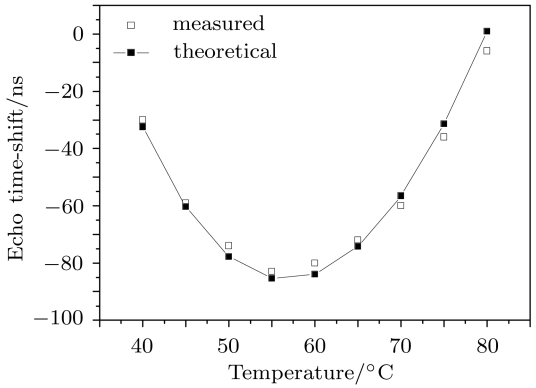

Fig.11. The relationship between temperature and echo time-shift at the focus.

The averaged echo-strain at the focus is evaluated in the range of 37 to 80 °C as shown in Fig.12, where the theoretical estimation is denoted by the solid line, the measured values are denoted by solid squares, and the polynomial fit is represented by the dashed line. From this figure, we can find that the discrepancy between the results of theory and measurement is observed at temperatures higher than about 75 °C.

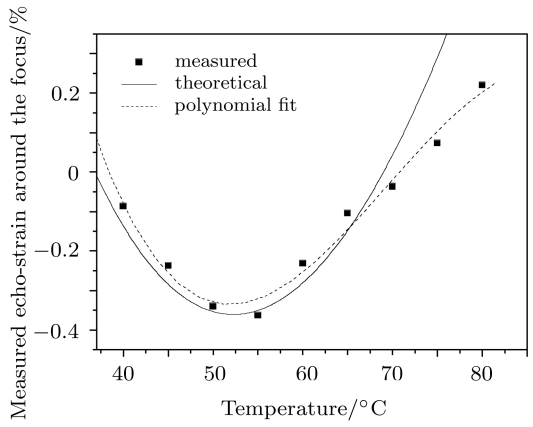

Fig.12. Echo-strain at the focus at different temperatures.

In light of the temperature dependence of echo-strain in Fig.2, we can evaluate the temperature from echo-strain as shown in Fig.13, where the theoretical temperatures are plotted as the solid line, and the estimated temperatures are denoted by open squares. It is found that the measured temperatures coincide well with those of the theoretical values, with the accuracy of ±2 °C in the range of 37 to 75 °C, but the error begins to increase as the temperature goes above 75°C.

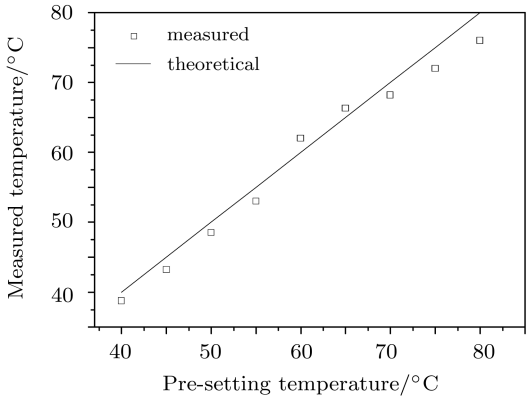

Fig.13. Estimated temperatures at the focus from echo-strain.

5. Conclusion

Noninvasive temperature estimation in therapeutic ultrasound treatment is a hotspot in current research field of ultrasound therapy. In this paper, we have discussed the feasibility of noninvasive temperature estimation by detecting the echo-strain along with thermal expansion of the tissue. Computer simulation and preliminary experimental studies are performed using porcine liver tissue in the temperature range of 37–80 °C. Results indicate that this technique can detect temperatures below 75 °C with an accuracy of ±2 °C, effectively expanding the detected temperature range measured by the time-shift technique. It should be noted that there exist some differences between our measurement and the real configuration in ultrasound therapeutic system, for example, the influence of blood stream and respiration. Additionally, further assessment of this technique of using ultrasonic heating is required.

References

[1] ter Haar G, Sinnett D and Rivens I 1989 *Phys. Med. Biol.* **34** 1743

[2] ter Harr G 1995 *Ultrasound in Med. & Biol.* **21** 1989

[3] Lu Y, Liu X Z, Gong X F and Zhang D 2004 *Chinese Science Bulletin* **49** 2360

[4] Damaianou C, Pavlou M, Velev O, Kyriakou K and Trimikliniotis M 2004 *Ultrasound in Med. & Biol.* **30** 397

[5] Seip R, VanBaren P, Cain C and Ebbini E S 1996 *IEEE Trans. Ultrason. Ferroelect. Freq. Contr.* **43** 1063

[6] Miller N R, Bamber J C and Meaney P M 2002 *Ultrasound in Med. & Biol.* **28** 1319

[7] Souchon R, Bouchoux G, Maciejko E, Lafon C, Cathignol D, Bertrand M and Chapelon J Y 2005 *Ultrasound in Med. & Biol.* **31** 251

[8] Maass-Moreno R and Damianou C A 1996 *J. Acoust. Soc. Am.* **100** 2514

[9] Maass-Moreno R, Damianou C A and Sanghvi N T 1996 *J. Acoust. Soc. Am.* **100** 2522

[10] Techavipoo U, Varghese T, Zagzebski J A, Stiles T and Frank G 2002 *Ultrason. Imaging* **24** 246

[11] Kallel F, Stafford R J, Price R E, Righetti R, Ophir J and Hazle J D 1999 *Ultrasound in Med. & Biol.* **25** 641

[12] Sehgal C M, Brown G M, Bahn R C and Greenleaf J F 1986 *Ultrasound in Med. & Biol.* **12** 865

[13] Kuznetsov V 1970 *Sov. Phys. Acoust.* **16** 467

[14] Zhu X F, Zhou L, Zhang D and Gong X F 2005 *Chin. Phys.* **14** 1594

[15] Pennes H H 1948 *J. Appl. Physiol.* **1** 193

[16] Qian S Y and Wang H Z 2001 *Acta Phys. Sin.* **50** 501 (in Chinese)

[17] Jensen J A 1996 *Med. Bio. Eng. Computing* **34** (Suppl. 1) 351

[18] Lizzi F L, Muratore R, Deng C X, Ketterling J A, Alam S K, Mikaelian S M and Kalisz A 2003 *Ultrasound in Med. & Biol.* **29** 1593